A validated analytical model for a cyclorotor wave energy device

Andrei Ermakov, John V. Ringwood

Abstract—We present a new analytical model for a horizontal axis cyclorotor-based wave energy converter (WEC). A number of cyclorotor-based WEC concepts and models, with different numbers of hydrofoils, have previously been studied. Our model is derived for a horizontal cyclorotor with 2 hydrofoils. The governing equations are optimised and converted to the polar coordinate system. The mechanical model is based on Newton's second law for rotation. Rotation is considered in two-dimensional potential flow, for both monochromatic and panchromatic waves, including waves generated by the rotating rotor, and viscous losses. The developed model is very convenient for modelling, analysis and control design for a cyclorotor based WEC.

The authors of this work have derived new, exact, analytic functions for the free surface perturbation and induced fluid velocity field caused by hydrofoil rotation. These new formulae significantly decrease the model calculation time, compared to previous models, and increase the accuracy of the results. We present the results of free rotation simulations for the rotor in monochromatic and panchromatic waves obtained with the use of the newly derived equations.

Index Terms—Control design, Cyclorotor, Rotor, LiftWEC, Wave Energy Converter

I. INTRODUCTION

Wave energy is one of the few untapped sources of renewable energy that could make a significant contribution to the future energy system. Unfortunately, to date, none of the more traditional prototypes which use buoyancy or diffraction wave forces have proven themselves to be commercially viable. This provides motivation for the development of new approaches to wave energy conversion. One of the recent and most promising methods is obtaining energy from the elliptical motion of water wave particles using a horizontal cyclorotor with hydrofoils. Even though this idea is more than 40 years old [1], few prototypes have ever been built and tested [2]–[4]. The authors of these concepts consider different types of cyclorotors with various numbers of hydrofoils. In this work, we

consider a mathematical model for a cyclorotor with 2 hydrofoils and present newly derived and validated formulae which can describe it.

The first prototype concept of a lift force based WEC, a rotor with a single hydrofoil, termed the Rotating Wing, was tested by Hermans et al. [2] in the deep water basin of MARIN. It was shown that the device rotates at the wave frequency and can absorb energy from waves. The authors also derived the first mathematical model of the cyclorotor-based WECs.

Significant work on the development of cyclorotor-based WECs was conducted by the Atargis Energy Corporation [5]. The proposed Cycloidal Wave Energy Converter (CycWEC) is a cyclorotor with two hydrofoils. This concept was tested as a 1:300 scale prototype, in a 2D wave tunnel of the US Air Force Academy [6]–[8] and as a 1:10 model in a 3D wave tank at the Texas A&M Offshore Technology Research Center [9], [10]. The wide range of publications [5]–[10] outline the evolution of the proposed CycWEC numerical model and increase of its accuracy.

Cyclorotor based WECs were also studied in the PhD thesis of Scharmann [3]. Experiments were conducted in the Hamburg Ship Model Basin, Germany. The author proposed the concept of a cyclorotor with 4 hydrofoils and a straight-forward robust control scheme as the most promising approach. The numerical modelling of this cyclorotor is based on the commercial software Ansys Fluent and OpenFOAM.

Reviews of cyclorotor-based WECs conducted by different authors [3], [11], [12] have shown that a cyclorotor may have a wide range of possible configurations, operational principles, actuators, and may be suitable for different strategies of wave energy extraction. A classification of lift-force-based WECs proposed by Folley and Whittaker [11] is based on the specific method of generating lift and the motion of the body. The work reported in [11] provided the inspiration for the LiftWEC project [13], which is also dedicated to cyclorotor-based WEC development.

In this article we present a new analytical model, which is derived for a horizontal cyclorotor with two hydrofoils in the polar coordinate system. It is relatively simple, fast, and suitable for analytical and numerical study of cyclorotor based WECs, as well as control system development. This was achieved by using new analytical formulae, which were derived by the authors and validated with numerical and experimental results published in previous research [5]. These new formulae significantly decrease the calculation time, compared to previous models [2], [4], and increase the accuracy of the results, as well as

providing useful insight into the nature of the system behaviour.

The remainder of the paper is organised as follows: §II of this article is dedicated to the mechanical model and contains a detailed diagram of the cyclorotor. In §III, we describe the hydrodynamic model, present new formulae for the waves generated by rotating hydrofoils and their validation with the results presented in previous research. In §IV we introduce the point source model for a hydrofoil and present new exact formulae which can describe a cyclorotor with two hydrofoils in the polar coordinate system. In §V numerical results of the simulations free cyclorotor rotating in monochromatic and panchromatic waves. In conclusion, we sum up the obtained results and discuss perspectives of the model in the study of cyclorotor-based WECs.

II. THE MECHANICAL MODEL

We consider wave propagation in the Cartesian coordinate system, and rotor rotation in polar coordinates, as shown in Fig. 1. The rotational centre of the cyclorotor is located at $x_0 = 0$ and submerged by y_0.
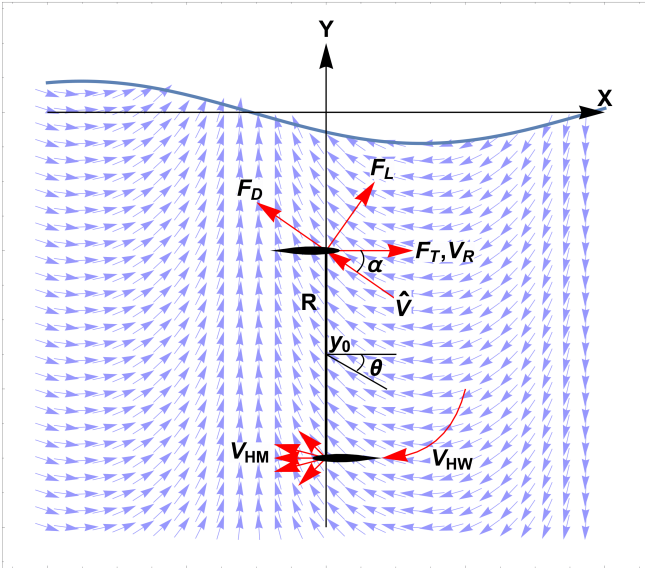

Fig. 1. The detailed diagram of the cyclorotor with two hydrofoils: θ - polar coordinates of the hydrofoils, V_W - wave induced fluid velocity, V_R - speed of the foils, V_{HM} - instantaneous radiation from the moving foil and V_{HW} - the wake which is left behind, $\hat{V}$ - the overall relative to hydrofoil fluid velocity, α - the attack angle, F_L, F_D, F_T - lift, drag and tangential forces.

The position of the hydrofoils can be determined as:

$$x_i(t) = -R\cos(\theta(t) + \pi i) \qquad (1)$$
$$y_i(t) = y_0 + R\sin(\theta(t) + \pi i) \qquad (2)$$

where $i = 1, 2$ is the hydrofoil number, (x_i, y_i) is the position of hydrofoil i, R is the operational radius, and $\theta(t)$ is the polar angle coordinate in the selected time moment t.

Taking the time derivatives of the positions (1,2), we can obtain the velocity vectors of the foils $\vec{V_R} = \{(V_R)_x, (V_R)_y\}$ as:

$$(V_{R_i})_x = R\dot{\theta}(t)\sin(\theta(t) + \pi i) \qquad (3)$$
$$(V_{R_i})_y = R\dot{\theta}(t)\cos(\theta(t) + \pi i) \qquad (4)$$

where $\dot{\theta}(t)$ is the angular velocity.

The mechanical model of the rotor is based on Newton's second law for rotation and balances the product of the rotor's acceleration $\ddot{\theta}(t)$ and inertia I with the torques caused by the tangential forces F_{T_i} generated on the hydrofoils. It is assumed that the model is directly connected with a rotational generator, which exerts an opposing torque, $\mathcal{T}$:

$$I\ddot{\theta}(t) = (F_{T_1} + F_{T_2})R - \mathcal{T} \qquad (5)$$

The tangential forces F_{T_i} generated on the hydrofoil can be manipulated by pitching the hydrofoils which, in turn, changes the attack angle α. The PTO torque $\mathcal{T}$ is used both to take rotational energy from the system, to generate electrical energy, or supply energy to increase rotational speed. In the second case, we presume the PTO generator system has the ability to switch to a motoring mode.

As an example performance function, we use captured energy in a traditional form used in wind, tidal and wave energy metrics. It is defined as maximisation of the time integral of the product between angular velocity $\dot{\theta}(t)$ and PTO torque on the time interval $[0, T]$.

$$Max \quad J = \int_0^T \mathcal{T}(t)\dot{\theta}(t)dt \qquad (6)$$

In this particular study, we examine only the free rotation response of the system ($\mathcal{T}(t) = 0$), but include the possibility in (5) since one of the target uses for the developed model is as a platform for model-based control design.

III. THE HYDRODYNAMIC MODEL

We consider rotation in two-dimensional potential flow which includes incoming monochromatic or panchromatic waves, as well as radiated waves generated by the rotating rotor, and viscous losses.

As an example of incoming waves, we present Airy waves which were used in the study of Siegel et al [14], and can be described by the following velocity potential:

$$\Phi_W(x, y, t) = \frac{Hg}{2\omega}e^{ky}\sin(kx - \omega t) \qquad (7)$$

where H is a wave height, ω is wave frequency, k is wave number, and g is the acceleration due to gravity.

The components of the wave induced velocity can be found as a gradient from the potential:

$$\mathbf{V_w} = \nabla\Phi_W(x, y, t) = \left\{(V_W)_x, (V_W)_y\right\} \qquad (8)$$

After the substitution of the coordinates (3,4), we can define the wave induced velocity which acts on hydrofoil i at time t, as:

$$(V_{W_i})_x = \frac{e^{ky_i}gHk}{2\omega}\cos(kx_i - t\omega) \qquad (9)$$
$$(V_{W_i})_y = \frac{e^{ky_i}gHk}{2\omega}\sin(kx_i - t\omega) \qquad (10)$$

One of the challenges in the development of a cyclorotor-based WEC is estimation of the waves radiated by rotating hydrofoils. In previous work [2]–[4], the hydrofoil, from the far-field, was modelled as a single moving point vortex in infinitely deep water. This vortex can be represented by a complex potential which satisfies the kinematic and dynamic boundary condition on the free surface [15]:

$$
F(z,t) = \frac{\Gamma(t)}{2\pi \mathtt{i}} Log \left[\frac{z - c(t)}{z - \tilde{c}(t)} \right] +
$$
$$
\frac{g}{\pi \mathtt{i}} \int_0^t \int_0^\infty \frac{\Gamma(\tau)}{\sqrt{gk}} e^{-\mathtt{i}k(z-\tilde{c}(\tau))} \sin\left(\sqrt{gk}(t-\tau) \right) dk d\tau \tag{11}
$$

where $z = x + \mathtt{i}y$ is the complex coordinate, $c(t) = x_i(t) + \mathtt{i}y_i(t)$ is the position of the hydrofoil i, $\tilde{c}(t)$ is the complex conjugate of $c(t)$, k is the wave number, and $\Gamma(t)$ is the circulation of the vortex, or the line integral of the fluid velocity along a closed path.

The potential $F(z,t)$ in (11) consists of two parts. The first term on the right-hand side of (11) is the instantaneous (momentary) radiation, which has a singularity at the source point $c(t)$. For this reason, it cannot be used to describe the state in the close vicinity of the foil. The second term on the right-hand side of (11) describes the fluid velocity wake caused by the moving vortex. In the study by Hermans et al. [2], this term is calculated numerically, using double integration over the wave number k and the time parameter τ. A very similar approach is employed in the work of Siegel et al. [14], where it was integrated using second order k and τ marching techniques.

The authors of this current work have solved the integral over k analytically in the form of the Dawson function $D[x]$ [16]:

$$
F(z,t) = \frac{\Gamma(t)}{2\pi \mathtt{i}} Log \left[\frac{z - c(t)}{z - \tilde{c}(t)} \right] -
$$
$$
\frac{2\mathtt{i}\sqrt{g}}{\pi} \int_0^t \frac{\Gamma(\tau)}{\sqrt{\mathtt{i}(z - \tilde{c}(\tau))}} D \left[\frac{\sqrt{g}(t-\tau)}{2\sqrt{\mathtt{i}(z - \tilde{c}(\tau))}} \right] d\tau \tag{12}
$$

where

$$
D[x] = e^{-x^2} \int_0^x e^{y^2} dy. \tag{13}
$$

This new formula significantly decreases the calculation time and increases the accuracy of the results.

The velocity of the waves radiated by a rotating hydrofoil can now be found using the following equation:

$$
\mathbf{V_H} = \frac{\partial F(z,t)}{\partial z} = (V_H)_x - \mathtt{i}(V_H)_y \tag{14}
$$

The velocity field $\mathbf{V_H}$ of the waves radiated by the hydrofoil also consists of the instantaneous radiated waves $\mathbf{V_{HM}}$ and wakes $\mathbf{V_{HW}}$ which were left in the hydrofoil's path:

$$
\mathbf{V_H} = \mathbf{V_{HM}} + \mathbf{V_{HW}} \tag{15}
$$

The complex potential $F(z,t)$ can also be presented in the form of the sum of the velocity potential Φ_H and stream function Ψ_H as:

$$
F(z,t) = \Phi_H(x,y) + \mathtt{i}\,\Psi_H(x,y) \tag{16}
$$

Thus, the new velocity potential (derived by the authors), for waves radiated by the hydrofoil, has the following form:

$$
\Phi_H(x,y) = \frac{\Gamma(t)}{2\pi} \arctan \left[\frac{2y_i\,(x_i - x)}{(x - x_i)^2 + (y^2 - y_i^2)} \right] +
$$
$$
\int_0^t \frac{\Gamma[\tau]\sqrt{g}}{\pi} \left(\frac{(-1)^{1/4} D \left[\frac{(-1)^{3/4}\sqrt{g}(t-\tau)}{2\sqrt{(x-x_i[\tau]) + \mathtt{i}(y+y_i[\tau])}} \right]}{\sqrt{(x-x_i[\tau]) + \mathtt{i}(y+y_i[\tau])}} + \right.
$$
$$
\left. \frac{(-1)^{3/4} D \left[\frac{(-1)^{1/4}\sqrt{g}(t-\tau)}{2\sqrt{(x-x_i[\tau]) - \mathtt{i}(y+y_i[\tau])}} \right]}{\sqrt{(x-x_i[\tau]) - \mathtt{i}(y+y_i[\tau])}} \right) d\tau \tag{17}
$$

and, despite the presence of the complex terms, the value of the function in (17) is always real.

In the case of the potential flow, the free surface perturbation can be found from the dynamic boundary condition. For example, the elevation of the free surface caused by the Airy wave has the following form:

$$
\eta_w = -\frac{1}{g} \left(\frac{\partial \Phi_W}{\partial t} \right)_{y=0} = \frac{H}{2} \cos(kx - \omega t) \tag{18}
$$

Now, we can obtain the perturbation of the free surface caused by rotating hydrofoil i using equation (17):

$$
\eta_{h_i} = -\frac{1}{g} \left(\frac{\partial \Phi_{H_i}}{\partial t} \right)_{y=0} \tag{19}
$$

and the overall elevation of the free surface can be presented in the form of the linear sum:

$$
\eta = \eta_w + \eta_{h_1} + \eta_{h_2} \tag{20}
$$

We validate the results obtained using equations (17) and (19), for the heights and periods of the waves generated by a single rotating hydrofoil, against results obtained experimentally and numerically by previous researchers [17], [18].

Here, we present a comparison with the numerical simulation presented in [14]. The authors of this paper have simulated single hydrofoil rotor rotation in still water and evaluated the elevation of the free surface at a measurement point located downstream. The parameters were normalised by a period of $T = 9$ s and wave length $\lambda_{Airy} = 126.5$ m. The single hydrofoil rotor has radius $R/\lambda_{Airy} = 0.15$, submergence depth $|y_0|/\lambda_{Airy} = 0.18$, and circulation $\Gamma T/\lambda_{Airy}^2 = 5.6 \cdot 10^{-3}$. All waves are evaluated at x = $3\lambda_{Airy}$ and at time t/T = 30 after the start of the cycloidal WEC. We have extracted the simulation data from the figures presented in article [14] with the use of the Graphreader software [19].

The numerical results obtained in [14] are presented in Fig. 2 (red line) are in good agreement with our
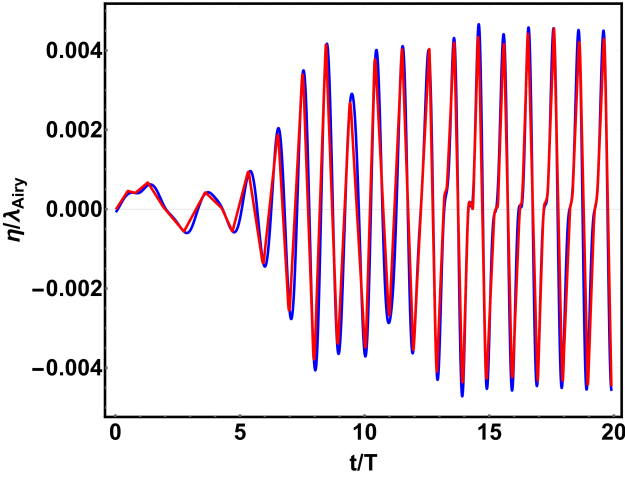
Fig. 2. The elevation of the free surface at the measurement point located downstream upstream: obtained with the use of new equation - blue line, (b) obtained from the numerical simulations presented in [14] - red line

numerical results (blue line). The higher amplitudes of the free surface perturbations can be explained by more accurate calculation in comparison with the previous research, where only limited amount of radiated wave numbers k were considered. The derived equations (17) can also be beneficial for the calculation of the most recent performance metrics proposed in [4] which are based on the wave radiation and cancellation effects.

IV. POINT SOURCE REPRESENTATION

We use a basic representation of the hydrofoils as point sources. For this case, the lift and drag coefficients should be considered not as physical values, but more as tuning parameters. These best-fit approximate coefficients can be obtained from numerical simulations or experimental tests. These parameters depend on the following system inputs, which can be measured or tracked in real time:

1) The wave induced fluid velocity $\mathbf{V_W}$ can be reliably predicted in real time due to the minimal upstream radiation [2], [7]
2) The rotational velocity $\mathbf{V_R}$, and position of the rotor θ, can be measured and controlled [6]
3) The velocity of the waves radiated by the hydrofoils $\mathbf{V_H}$ can be calculated relatively easily; however, we cannot define the instantaneous radiated waves $(\mathbf{V_{HM}})_i$ in the vicinity close to the point source i, due to the singularity highlighted in [14].

Thus, we consider the generation of the lift and drag forces as the result of the rotation of the hydrofoil i with an $\hat{\mathbf{V}}_i$, representing the vector difference between the wave induced fluid velocity $\mathbf{V_{W_i}}$ and the cyclorotor rotational velocity $\mathbf{V_{R_i}}$, plus the sum of the wakes caused by the hydrofoil rotation $\mathbf{V_{HW}}$ and instantaneous radiation from the other foils $\mathbf{V_{HM}}$ as:

$$\hat{\mathbf{V}}_i = \mathbf{V_{W_i}} - \mathbf{V_{R_i}} + \mathbf{V_{HW_i}} + \mathbf{V_{HM_j}} + \mathbf{V_{HW_j}} \quad (21)$$

Then the squared modulus of the value overall relative velocity can be found as:

$$|\hat{\mathbf{V}}_i|^2 = (\hat{V}_i)_x^2 + (\hat{V}_i)_y^2 \quad (22)$$

It is more convenient to present a two dimensional problem using polar coordinates. Below, we introduce the set of coefficients which are used for simplification of the projection components of the relative velocity.

$$
\begin{aligned}
M_1 &= -2y_0 + R\sin(\theta) + R\sin(\theta(\tau)) + \\
&\quad \mathtt{i}R\cos(\theta) - \mathtt{i}R\cos(\theta(\tau)) \\
M_2 &= -2y_0 + R\sin(\theta) - R\sin(\theta(\tau)) + \\
&\quad \mathtt{i}R\cos(\theta) + \mathtt{i}R\cos(\theta(\tau)) \\
M_3 &= -2y_0 - R\sin(\theta) - R\sin(\theta(\tau)) - \\
&\quad \mathtt{i}R\cos(\theta) + \mathtt{i}R\cos(\theta(\tau)) \\
M_4 &= -2y_0 - R\sin(\theta) + R\sin(\theta(\tau)) - \\
&\quad \mathtt{i}R\cos(\theta) - \mathtt{i}R\cos(\theta(\tau))
\end{aligned}
$$
$$(23)$$

The parameter $\tilde{\tau} = \sqrt{g}(t - \tau)$ is also used for simplification, so that:

$$
\begin{aligned}
\left(\hat{V}_1\right)_x &= R\dot\theta\sin(\theta) + \\
&\frac{gHk}{2\omega}e^{k(y_0 - R\sin(\theta))}\cos(\omega t - kR\cos(\theta)) + \\
&\frac{\Gamma_2}{4\pi}\left(\frac{y_0}{y_0^2 + R^2\cos^2(\theta)} + \frac{\sin(\theta)}{R}\right) + \\
&Re\left[\frac{\sqrt{g}}{2\pi}\int_0^t \frac{\Gamma_1(\tau)}{M_1^{5/2}}\left(D\left[\frac{\tilde\tau}{2\sqrt{M_1}}\right](\tilde\tau^2 - 2M_1) - \tilde\tau\sqrt{M_1}\right) + \right.\\
&\left.\frac{\Gamma_2(\tau)}{M_2^{5/2}}\left(D\left[\frac{\tilde\tau}{2\sqrt{M_2}}\right](\tilde\tau^2 - 2M_2) - \tilde\tau\sqrt{M_2}\right)d\tau\right], \quad (24)
\end{aligned}
$$

$$
\begin{aligned}
\left(\hat{V}_1\right)_y &= R\dot\theta\cos(\theta) - \\
&\frac{gHk}{2\omega}e^{k(y_0 - R\sin(\theta))}\sin(\omega t - kR\cos(\theta)) + \\
&\frac{\Gamma_2\cos(\theta)}{4\pi R}\left(\frac{y_0^2 - R^2\sin^2(\theta)}{y_0^2 + R^2\cos^2(\theta)}\right) - \\
&Im\left[\frac{\sqrt{g}}{2\pi}\int_0^t \frac{\Gamma_1(\tau)}{M_1^{5/2}}\left(D\left[\frac{\tilde\tau}{2\sqrt{M_1}}\right](\tilde\tau^2 - 2M_1) - \tilde\tau\sqrt{M_1}\right) + \right.\\
&\left.\frac{\Gamma_2(\tau)}{M_2^{5/2}}\left(D\left[\frac{\tilde\tau}{2\sqrt{M_2}}\right](\tilde\tau^2 - 2M_2) - \tilde\tau\sqrt{M_2}\right)d\tau\right], \quad (25)
\end{aligned}
$$

$$
\begin{aligned}
\left(\hat{V}_2\right)_x &= -R\dot\theta\sin(\theta) + \\
&\frac{gHk}{2\omega}e^{k(y_0 + R\sin(\theta))}\cos(\omega t + kR\cos(\theta)) + \\
&\frac{\Gamma_1}{4\pi}\left(\frac{y_0}{y_0^2 + R^2\cos^2(\theta)} - \frac{\sin(\theta)}{R}\right) + \\
&Re\left[\frac{\sqrt{g}}{2\pi}\int_0^t \frac{\Gamma_2(\tau)}{M_3^{5/2}}\left(D\left[\frac{\tilde\tau}{2\sqrt{M_3}}\right](\tilde\tau^2 - 2M_3) - \tilde\tau\sqrt{M_3}\right) + \right.\\
&\left.\frac{\Gamma_1(\tau)}{M_4^{5/2}}\left(D\left[\frac{\tilde\tau}{2\sqrt{M_4}}\right](\tilde\tau^2 - 2M_4) - \tilde\tau\sqrt{M_4}\right)d\tau\right], \quad (26)
\end{aligned}
$$

$$\left(\hat{V}_2\right)_y = -R\,\dot{\theta}\cos(\theta)-$$
$$\frac{gHk}{2\omega}e^{k(y_0+R\sin(\theta))}\sin(\omega t+kR\cos(\theta))-$$
$$\frac{\Gamma_1\cos(\theta)}{4\pi R}\left(\frac{y_0^2+R^2\sin^2(\theta)}{y_0^2+R^2\cos^2(\theta)}\right)-$$
$$Im\left[\frac{\sqrt{g}}{2\pi}\int_0^t\frac{\Gamma_2(\tau)}{M_3^{5/2}}\left(D\left[\frac{\tilde{\tau}}{2\sqrt{M_3}}\right]\left(\tilde{\tau}^2-2M_3\right)-\tilde{\tau}\sqrt{M_3}\right)+\right.$$
$$\left.\frac{\Gamma_1(\tau)}{M_4^{5/2}}\left(D\left[\frac{\tilde{\tau}}{2\sqrt{M_4}}\right]\left(\tilde{\tau}^2-2M_4\right)-\tilde{\tau}\sqrt{M_4}\right)d\tau\right]. \quad (27)$$

Each projection component of the overall relative velocity $\hat{V}_i$ is presented as a sum where the first term is the rotational velocity V_R, the second term is the wave induced velocity V_{W_i}, and the third term is the velocity of the instantaneous radiated waves from the opposite hydrofoil V_{HM}. The last two terms under the integral describe the fluid velocity wakes V_{HW} which were left by the rotating hydrofoils.

The attack angle $\alpha_i(t)$ can be found as the angle between the cyclorotor rotational velocity V_{R_i} and overall relative velocity $\hat{V}_i$:

$$\alpha_i(t) = \arcsin\left(\frac{(V_{R_i})_x\,(\hat{V}_i)_y - (V_{R_i})_y\,(\hat{V}_i)_x}{|V_{R_i}||\hat{V}_i|}\right) + \gamma_i \quad (28)$$

where γ_i is the hydrofoil pitch angle, which can be adjusted in real time.

In this model, we use the following approximation: lift and drag forces which act on the selected hydrofoil depend on the lift and drag coefficients $C_L(\alpha)$ and $C_D(\alpha)$, respectively, hydrofoil chord length S, density of the fluid ρ and the value overall relative velocity $\hat{V}$ at the centre of the hydrofoil $\{x_i, y_i\}$, as:

$$(F_L)_i = C_L\,(\alpha_i)\,\frac{1}{2}\rho|\hat{V}_i|^2 S, \quad (29)$$

$$(F_D)_i = C_D\,(\alpha_i)\,\frac{1}{2}\rho|\hat{V}_i|^2 S \quad (30)$$

Then, the circulation members, Γ_i can be determined using the following equation:

$$\Gamma_i = C_L\,(\alpha_i)\,\frac{1}{2}|\hat{V}_i|S \quad (31)$$

The tangential F_T and radial F_R forces can now be calculated as a combination of the lift F_L and drag F_D forces:

$$(F_T)_i = F_L(\alpha_i)\sin(\alpha_i-\gamma_i) - F_D(\alpha_i)\cos(\alpha_i-\gamma_i) \quad (32)$$
$$(F_R)_i = F_L(\alpha_i)\cos(\alpha_i-\gamma_i) + F_D(\alpha_i)\sin(\alpha_i-\gamma_i) \quad (33)$$

where α is the attack angle, which can be corrected by pitching of the hydrofoils. This control input can decrease the influence of the drag and increase influence of the lift forces.

The presented mathematical model has been validated in terms of tangential and radial forces against recent experimental results [20], [21] which were obtained in the wave flume of École Centrale de Nantes

(ECN). The experimental test campaign of a two-dimensional model of a cyclorotor-based WEC concept, with one or two foils, was carried out in June and July 2021. The 2D model was designed, built, assembled and commissioned by ECN.

We present the validation results for case 143 from the experimental data [20], [21]. In this case, rotation of a single hydrofoil with pitch $\gamma = 4^o$ and chord length S=0.3m, in monochromatic waves, has been studied. The incoming waves have wave period T= 1.8s and wave height H=0.253m. The rotor radius is R=0.3m, and the rotor rotates with the wave frequency $\dot{\theta} = \omega$ and with a relative phase angle of 90°. Incoming waves were approximated by Airy functions (7-10), with experimentally obtained values of tangential $(F_T)_{exp}$ and radial $(F_R)_{exp}$ forces used to derive the approximate lift and drag coefficients C_L and C_D from:

$$\begin{bmatrix}(F_T)_{exp}\\(F_R)_{exp}\end{bmatrix} = \begin{bmatrix}\sin(\alpha_1-\gamma_1) & -\cos(\alpha_1-\gamma_1)\\\cos(\alpha_1-\gamma_1) & \sin(\alpha_1-\gamma_1)\end{bmatrix}\cdot$$
$$\cdot\begin{bmatrix}C_L(\alpha_1)\\C_D(\alpha_1)\end{bmatrix}\cdot\frac{1}{2}\rho|\hat{V}_1|^2 S. \quad (34)$$

The system of (34) was enumerated at each of the experimental time steps (with a focus on a time interval from 77 to 98 s) and the approximate lift and drag coefficients derived and approximated using the method of least squares. While C_L and C_D are therefore tuned for these specific conditions, they provide acceptable agreement with the experimental data and simulate the changes of the tangential and radial for the foil which rotates in waves. The results of the simulations and their comparison with the experimental data are presented in Figs.3 and 4.
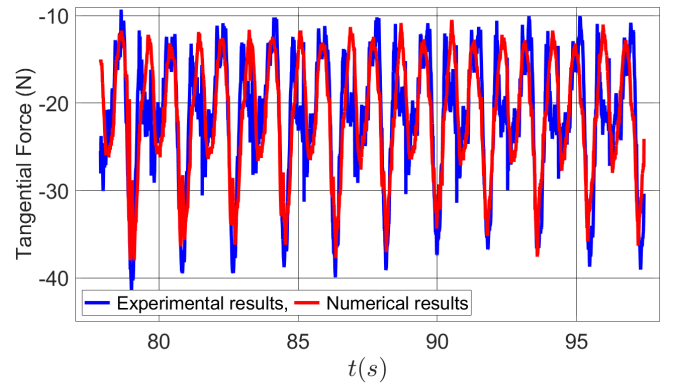

Fig. 3. Comparison of the experimental and numerical values of the tangential force
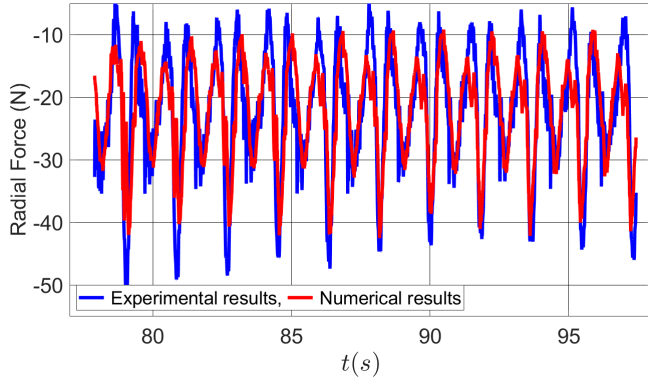
Fig. 4. Comparison of the experimental and numerical values of the radial force

V. NUMERICAL SIMULATIONS

In this section, we present the results of numerical simulations obtained with the use of the new model's equations outlined in Sections 2 and 4. As an example, we consider a rotor with two symmetric hydrofoils NACA0012, which is similar to the CycWEC prototype tested by Atargis in a 3D wave tank at the Texas A&M Offshore Technology Research Center [10]. The selected rotor has submergence depth y_0 = 2m, operational radius R = 1m, chord length S = 0.75m and inertia I = 500 kg m^2. The lift and drag coefficients used for the point source method were generated using XFLR5 software [22] for the symmetric hydrofoil NACA0012. Their values are presented on Fig. 5
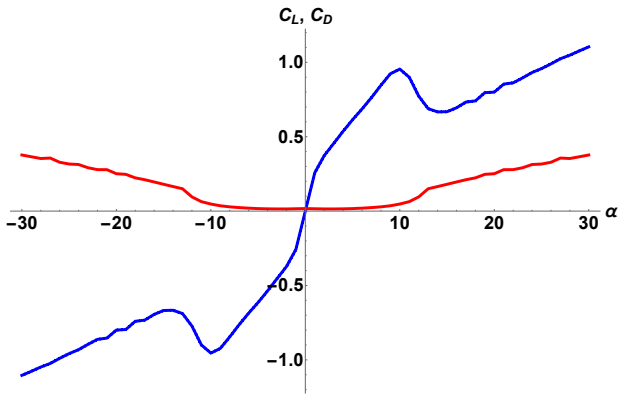

Fig. 5. The lift (blue line) and drag (red line) coefficients generated using XFLR5 software [22] for the symmetric hydrofoil NACA0012

A discrete time basis is considered and the time period T is separated into the set of n small intervals $\Delta t_i = \{t_i, t_{i+1}\}$. It is assumed that, at each small interval Δt_i, the rotational velocity $\dot{\theta}_i$ is constant. Then, the kinematic parameters of the rotor, at the next time step, can be defined as:

$$\theta_{i+1} = \theta_i + \dot{\theta}_i \Delta t_i + \ddot{\theta}_i \Delta t_i^2/2 \tag{35}$$
$$\dot{\theta}_{i+1} = \dot{\theta}_i + \ddot{\theta}_i \Delta t_i, \tag{36}$$
$$\ddot{\theta}_{i+1} = (\sum_{i=1}^{n} F_{Ti}[\Gamma_i, \theta_i, \dot{\theta}_i, \alpha_i] R - \mathcal{T}_i)/I \tag{37}$$

All calculations were conducted in Wolfram Mathematica using the forward difference method for differentiation and the trapezoidal rule for integration.

A. Case 1: Asymmetric rotor in monochromatic waves

In the first case, we consider the free motion in monochromatic waves with length λ = 9.75m, height H = 0.9 m and period T = 2.5 s. Initially, the hydrofoil rotor diameter is vertically aligned with the wave crest, i.e. $\theta(0) = \pi/2$, and the angular velocity is equal to the wave frequency, i.e. $\dot{\theta}(0) = \omega$. The considered rotor is asymmetric, with hydrofoil pitch angles $\gamma_1 = 5^o$ and $\gamma_2 = -5^o$. The result of the calculations are presented in Figs. 6 and 7.
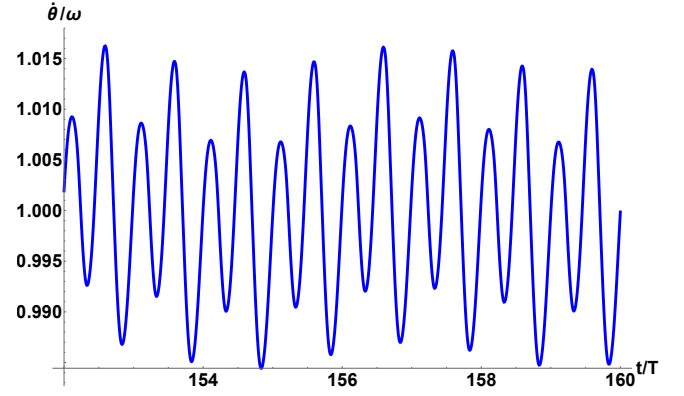

Fig. 6. The ratio between angular velocity and wave frequency for asymmetric rotor in monochromatic waves.
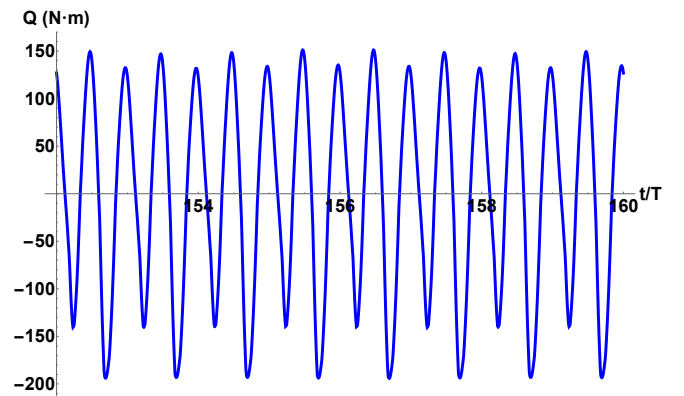

Fig. 7. The torque value fluctuation for asymmetric rotor in monochromatic waves.

Stable periodic rotation was achieved, and the rotor's periodic motion is synchronised with the incoming wave period T after 3 minutes. We can see that the angular velocity $\dot{\theta}$ has converged on the wave frequency ω. Significant fluctuation of the torque is visible.

B. Case 2: Symmetric rotor in monochromatic waves

In the second case, we consider the free rotation of the symmetric rotor with pitch angles $\gamma_1 = \gamma_2 = 0^o$ for the same ocean state considered in Case 1. The results of the calculations are shown on Figs. 8 and 9.

We can see that, after 3 minutes, the rotation frequency fluctuates in the vicinity of 2.925 times the waves' frequency. The higher rotational speed is caused by much greater values of the torque, the amplitude of which is also 3-4 times greater than the values obtained in the first case. This makes it impossible to achieve

convergence with the wave period. However the system's behaviour should eventually become periodic, but with much longer period than the wave period.
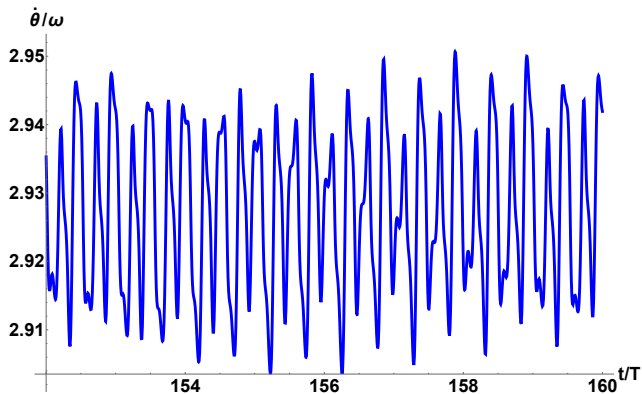

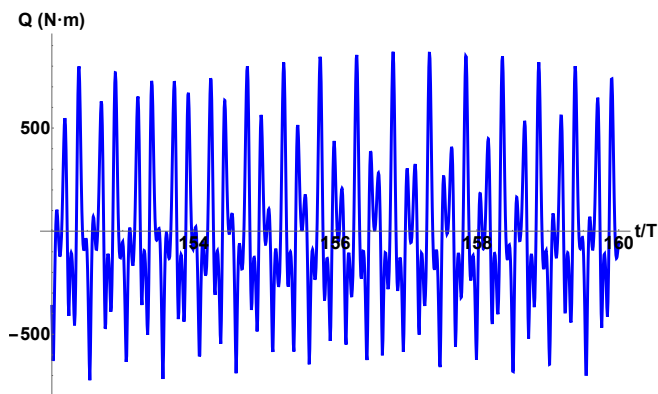Fig. 8. The ratio between angular velocity and wave frequency for symmetric rotor in monochromatic waves.

Fig. 9. The torque value fluctuation for symmetric rotor in monochromatic waves.

C. Case 3: Symmetric rotor in panchromatic waves

In the last example, we consider the free rotation of the symmetric rotor, with $\gamma_1 = \gamma_2 = 0^o$, in panchromatic waves. A JONSWAP spectrum is selected with wave significant height $H_s = 0.9$ m, period $T_s = 2.5$ s, peakiness parameter 5 and 80 discrete frequencies. In the conducted simulation, we consider the first 120 seconds from the start of the rotation. The free surface elevation above the cyclorotor centre $x = 0$ is presented in Fig. 10.

The obtained results show significant fluctuation of the rotation rate (see Fig. 11) and that the torque on the main shaft can reach very extreme values (see Fig. 12).

VI. CONCLUSION

The presented model can describe a cyclorotor-based WEC with various configurations, leading to its potential use in the optimisation of the rotor design. A number of simulations, which can be conducted with the use of this model, can help to determine the potential benefits of cyclorotor-based WECs and their perspective. However, it may require derivation of new lift and drag coefficients for the selected operational
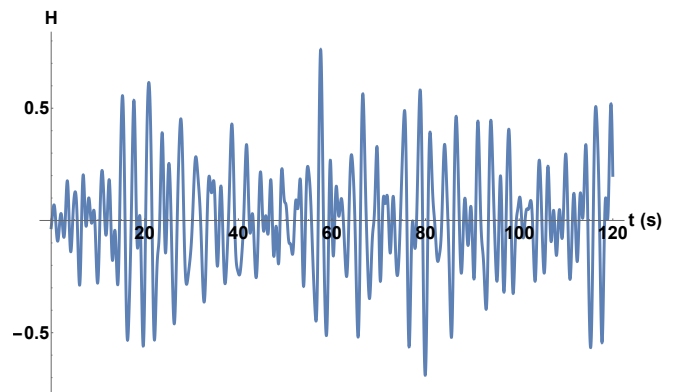

Fig. 10. The free surface elevation above the cyclorotors centre $x = 0$
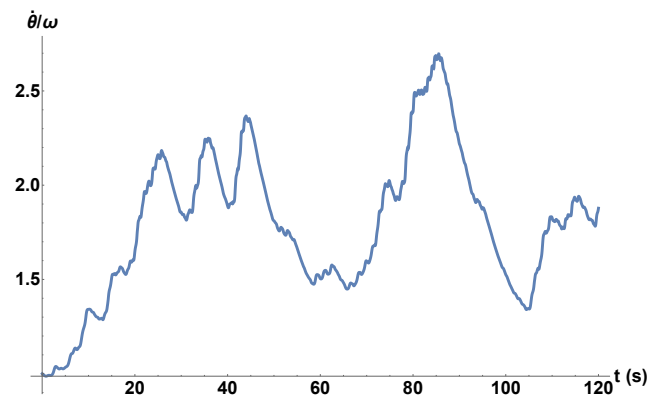

Fig. 11. The ratio between angular velocity and significant wave frequency $1/T_s$ for symmetric rotor in panchromatic waves.
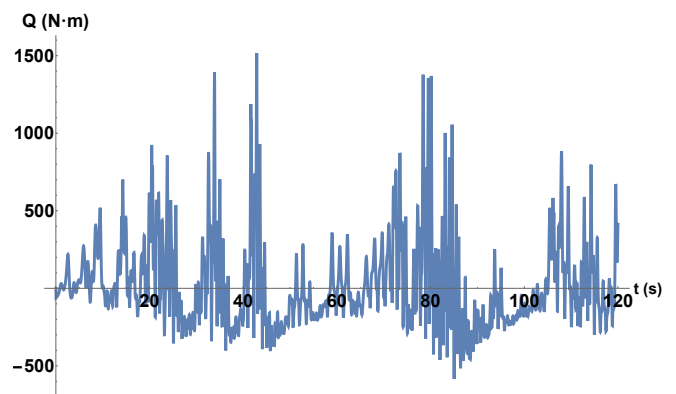

Fig. 12. The torque value fluctuation for symmetric rotor in panchromatic waves.

conditions. These coefficients could potentially be obtained from CFD simulations, or experimental results.

The developed model is validated and fast, lending itself to control design and implementation within model-based control schemes. For example, the point source model is suitable for model predictive control [23], since it takes approximately 4 seconds to calculate a 1-minute forecast, using Wolfram Mathematica. Customised coding would likely reduce this computational time by an order of magnitude. The newly derived exact analytical formulae for free surface elevation, and perturbation in fluid velocity, caused by a rotating foil can also help developers of existing, and new, cyclorotor concepts. The model is suitable for development of

various control strategies [24]–[26] which target different performance metrics, such as the wave cancellation proposed by Siegel et al. [4], or maximisation of the power coefficient (6) proposed by Scharmann [3].

REFERENCES

[1] M. McCormick, "Ocean wave energy concepts," in *Oceans'79*, 1979, pp. 553–558.

[2] A. J. Hermans, V. E. Sabben, and J. A. Pinkster, "A device to extract energy from water waves," *Applied Ocean Research*, vol. 12, no. 4, pp. 175–179, 1990.

[3] N. Scharmann, "Ocean energy conversion systems: the wave hydro-mechanical rotary energy converter." Ph.D. dissertation, Institute for Fluid Dynamics and Ship Theory, TUHH, Hamburg, Germany, 2014.

[4] S. Siegel, "Numerical benchmarking study of a cycloidal wave energy converter," *Renewable Energy*, vol. 134, pp. 390–405, 2019.

[5] Atargis Energy Corporation. CycWEC official website (accessed December 17, 2021). [Online]. Available: https://atargis.com//

[6] S. G. Siegel, M. Römer, J. Imamura, C. Fagley, and T. E. McLaughlin, "Experimental wave generation and cancellation with a cycloidal wave energy converter," in *Proceedings of the 30th international conference on offshore mechanics and arctic engineering*, Rotterdam, Netherlands, 2011.

[7] S. G. Siegel, C. Fagley, M. Römer, and T. McLaughlin, "Experimental investigation of irregular wave cancellation using a cycloidal wave energy converter," in *Proceedings of 31st international conference on ocean, offshore and arctic engineering*, Rio de Janeiro, Brazil, 2012.

[8] S. G. Siegel, C. Fagley, and S. Nowlin, "Experimental wave termination in a 2d wave tunnel using a cycloidal wave energy converter," *Applied Ocean Research*, vol. 38, pp. 92–99, 2012.

[9] C. Fagley, S. G. Siegel, and J. Seidel, "Wave cancellation experiments using a 1:10 scale cycloidal wave energy converter," in *Proceedings of 1st Asian wave and tidal conference series*, 2012.

[10] S. G. Siegel, *Cycloidal wave energy converter, Final scientific report: DOE Grant DE-EE0003635*, 2013.

[11] M. Folley and T. Whittaker, "Lift-based wave energy converters – an analysis of their potential," in *Proceedings of the 13th European Wave and Tidal Energy Conference*, Napoli, Italy, 2019.

[12] A. Ermakov and J. V. Ringwood, "Rotors for wave energy conversion — practice and possibilities," *IET Renewable Power Generation*, vol. 15, p. 3091–3108, 2021.

[13] LiftWEC official website (accessed December 17, 2021). [Online]. Available: https://liftwec.com/

[14] S. G. Siegel, T. Jeans, and T. E. McLaughlin, "Deep ocean wave energy conversion using a cycloidal turbine," *Applied Ocean Research*, vol. 33, no. 2, p. 110–119, 2011.

[15] J. V. Wehausen and E. V. Laitone, *Surface waves, Handbook of Physics, Vol. 9*, 1960.

[16] H. G. Dawson, "On the numerical value of $\int_0^h \exp(x^2)\,dx$," *Proceedings of the London Mathematical Society*, vol. s1-29 (1), pp. 519—-522, 1897.

[17] A. Ermakov and J. V. Ringwood, "A control-orientated analytical model for a cyclorotor wave energy device with n hydrofoils," *Journal of Ocean Engineering and Marine Energy*, vol. 7, no. 2, pp. 201–210, 2021.

[18] ——, "Erratum to: A control-orientated analytical model for a cyclorotor wave energy device with n hydrofoils," *Journal of Ocean Engineering and Marine Energy*, vol. 7, no. 4, p. 493–494, 2021.

[19] Graphreader is a tool to extract values from graph images (accessed December 17, 2021). [Online]. Available: http://www.graphreader.com/

[20] F. Thiebaut, G. Payne, S. Haquin, M. Web, S. Lambert, and B. Pettinotti. Liftwec project: D4.3 open access experimental data from 2d scale model. (accessed december 17, 2021). [Online]. Available: https://doi.org/10.5281/zenodo.5534471

[21] F. Thiebaut and G. Payne. Liftwec project: D4.4 report on physical modelling of 2d liftwec concepts. (accessed december 17, 2021). [Online]. Available: https://liftwec.com/d4-4-report-on-physical-modelling-of-2d-liftwec-concepts/

[22] The analysis tool for airfoils (accessed December 17, 2021). [Online]. Available: http://www.xflr5.tech/xflr5.htm

[23] N. Faedo, S. Olaya, and J. Ringwood, "Optimal control, mpc and mpc-like algorithms for wave energy systems: an overview," *IFAC Journal of Systems and Control*, vol. 1, pp. 37–56, 2017.

[24] J. Ringwood and A. Ermakov, "Energy-maximising control philosophy for a cyclorotor wave energy device," in *Proceedings of 41st international conference on ocean, offshore and arctic engineering*, Hamburg, Germany, 2022.

[25] A. Ermakov, A. Marie, and J. V. Ringwood, "Some fundamental results for cyclorotor wave energy converters for optimum power capture," *IEEE Transactions on Sustainable Energy*, vol. 13, no. 3, pp. 1869–1872, 2022.

[26] ——, "Optimal control of pitch and rotational velocity for a cyclorotor wave energy device," *IEEE Transactions on Sustainable Energy*, vol. 13, no. 3, pp. 1631–1640, 2022.